Electronic Supplementary Material (ESI) for Nanoscale.

Encapsulation of Ni/Fe_3O_4 heterostructures inside onion-like N-doped carbon nanorods enables synergistic electrocatalysis for water oxidation

Guang Liu[1,2], Rui Yao[1], Yong Zhao[1], Muheng Wang[1], Na Li[1], Yibing Li[2], Xin Bo[2], Jinping Li[1*], Chuan Zhao[2*]

1. Shanxi Key Laboratory of Gas Energy Efficient and Clean Utilization, Research Institute of Special Chemicals, Taiyuan University of Technology, Taiyuan, Shanxi 030024, PR China.
2. School of Chemistry, The University of New SouthWales, Sydney, New SouthWales 2052, Australia.

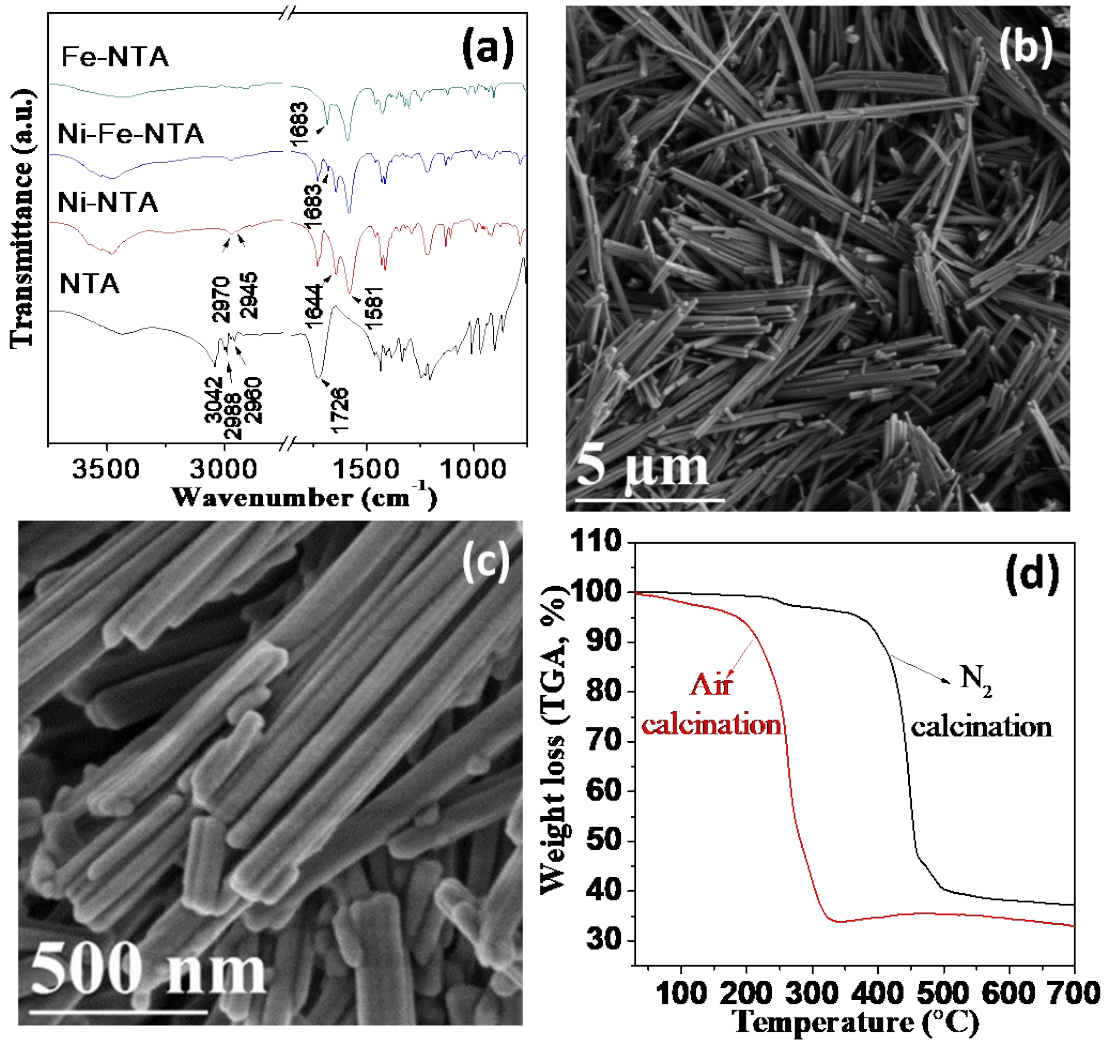

Figure S1. (a) FT-IR spectrum of NTA, Ni-NTA, NiFe-NTA and Fe-NTA; (b-c) SEM images of NiFe-NTA precursor; (d) TG curves of NiFe-NTA precursor under air and N_2 atmosphere.

FT-IR analysis demonstrated that the wide peak ranging from 3100 to 2900 cm^{-1} (3042, 2988, 2960 cm^{-1}), the band centering at 1726 cm^{-1}, and 1220 cm^{-1} for NTA can be ascribed to the stretching vibration of C-H, C=O and C-N chemical bonds, respectively. While for the NTA-complex compounds, due to the coordination of Ni (II) and/or Fe (II) with NTA, the peaks locate in 3042, 2988, 2960 cm^{-1} are moved to 2970, 2945 cm^{-1}. For Ni-NTA precursor, the peak of 1726 cm^{-1} becomes weak and a wide band composed of 1644, 1581 cm^{-1} is observed, implying the coordinated carboxylate group of Ni in Ni-NTA. While for Fe-NTA precursor, the peak of 1726 cm^{-1} is absent and replaces with two new peaks at 1683 and 1581 cm^{-1}, which also demonstrating the coordinated mode in Fe-NTA is differ from that of Ni-NTA. Moreover, the characteristic peak at 1725, 1683, 1644, and 1581 cm^{-1} of ν(C=O) for NiFe-NTA precursors were present, further proving the successful coordination of Ni (II) and Fe (II) with NTA in the Ni-Fe-NTA precursors.

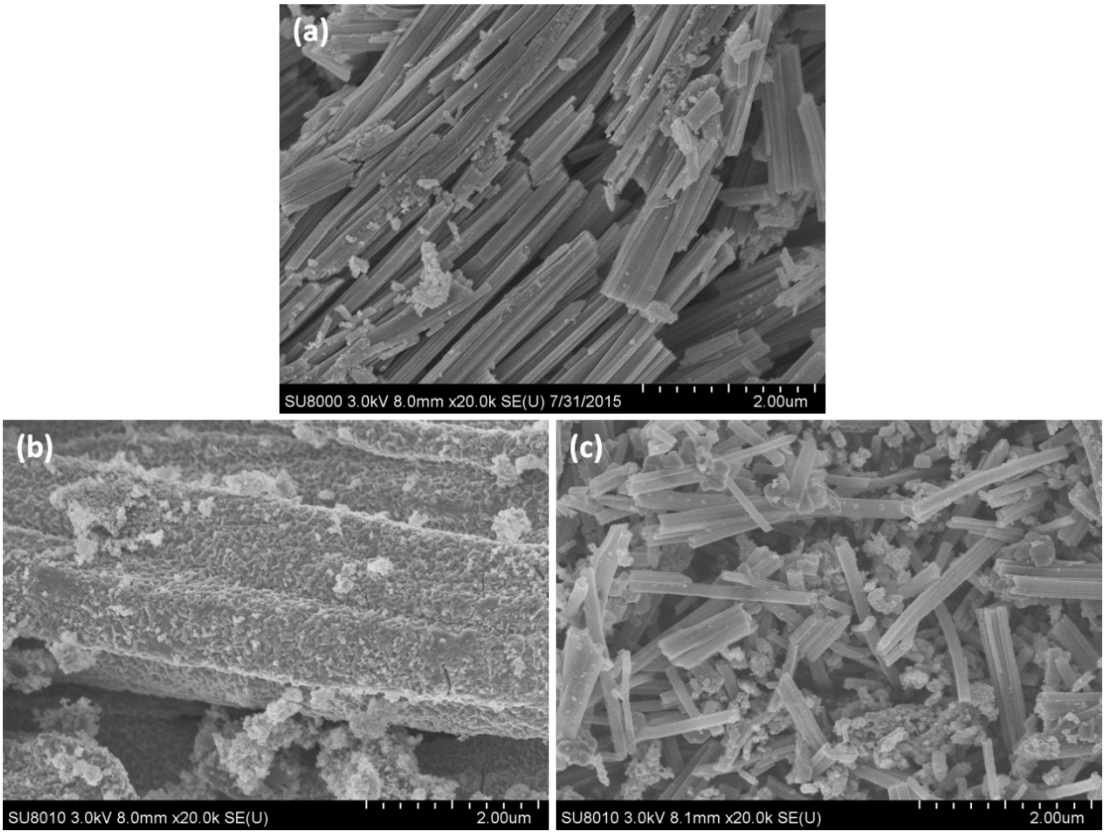

Figure S2. SEM images of (a) $NiFe_2O_4$; (b) Ni@ONC and (c) Fe_3O_4@ONC nanorods.

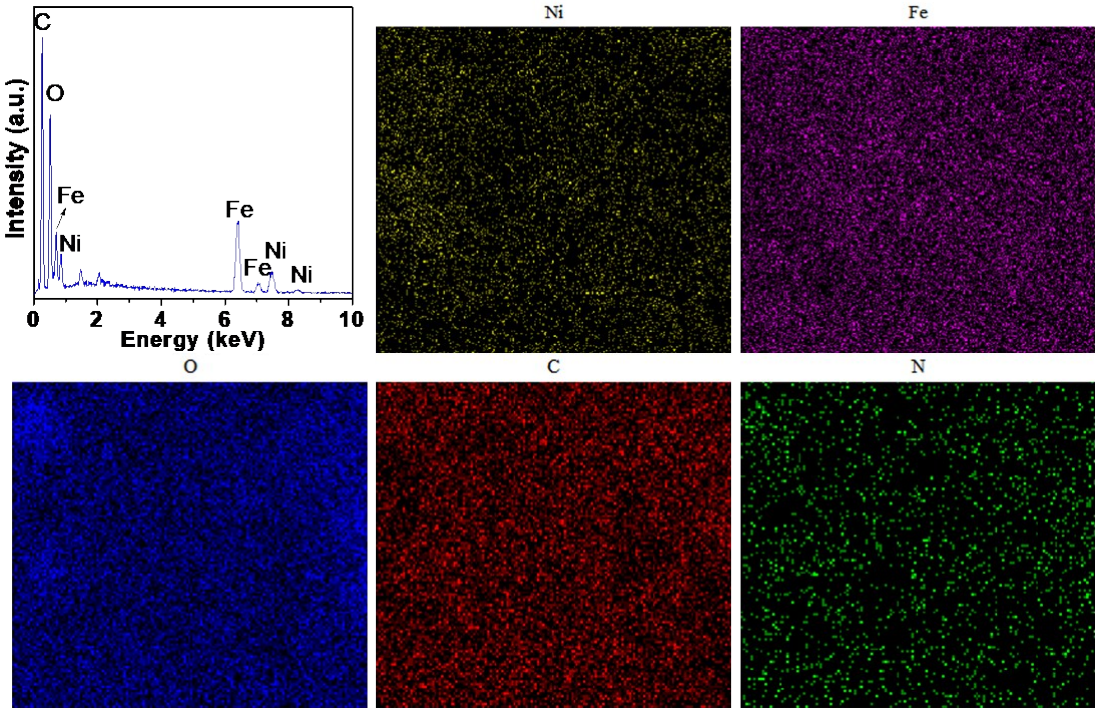

Figure S3. EDS curve and corresponding elemental mapping of Ni/Fe_3O_4@ONC nanorods.

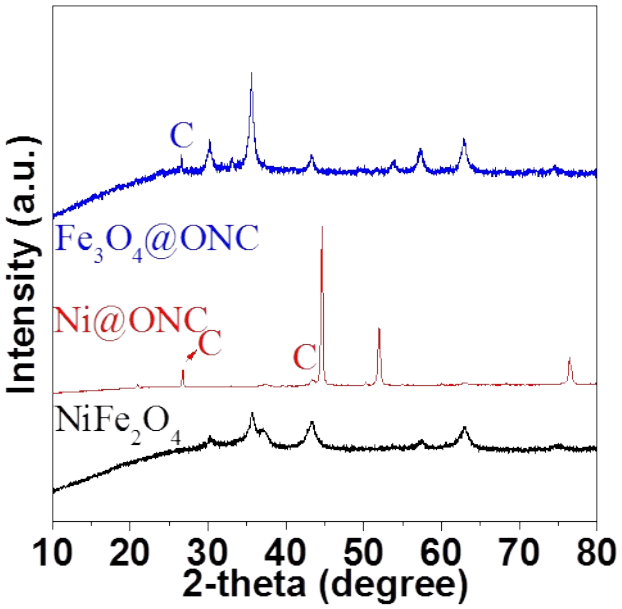

Figure S4. XRD patterns of $NiFe_2O_4$, Ni@ONC and Fe_3O_4@ONC nanorods.

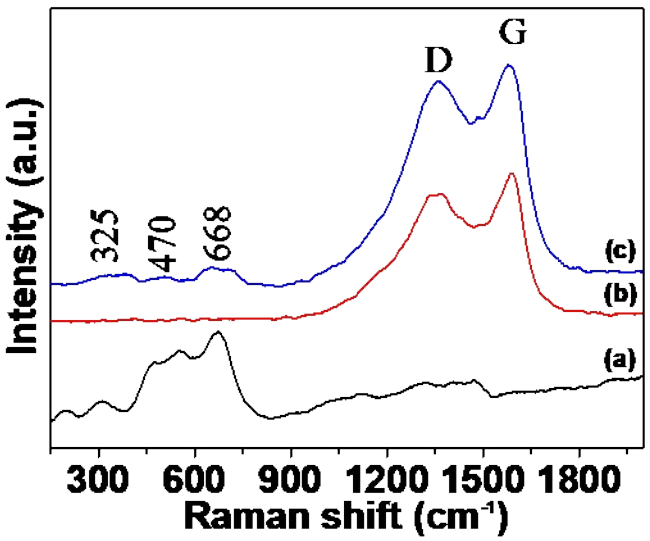

Figure S5. Raman spectra of (a) $NiFe_2O_4$; (b) Ni@ONC and (c) Fe_3O_4@ONC nanorods.

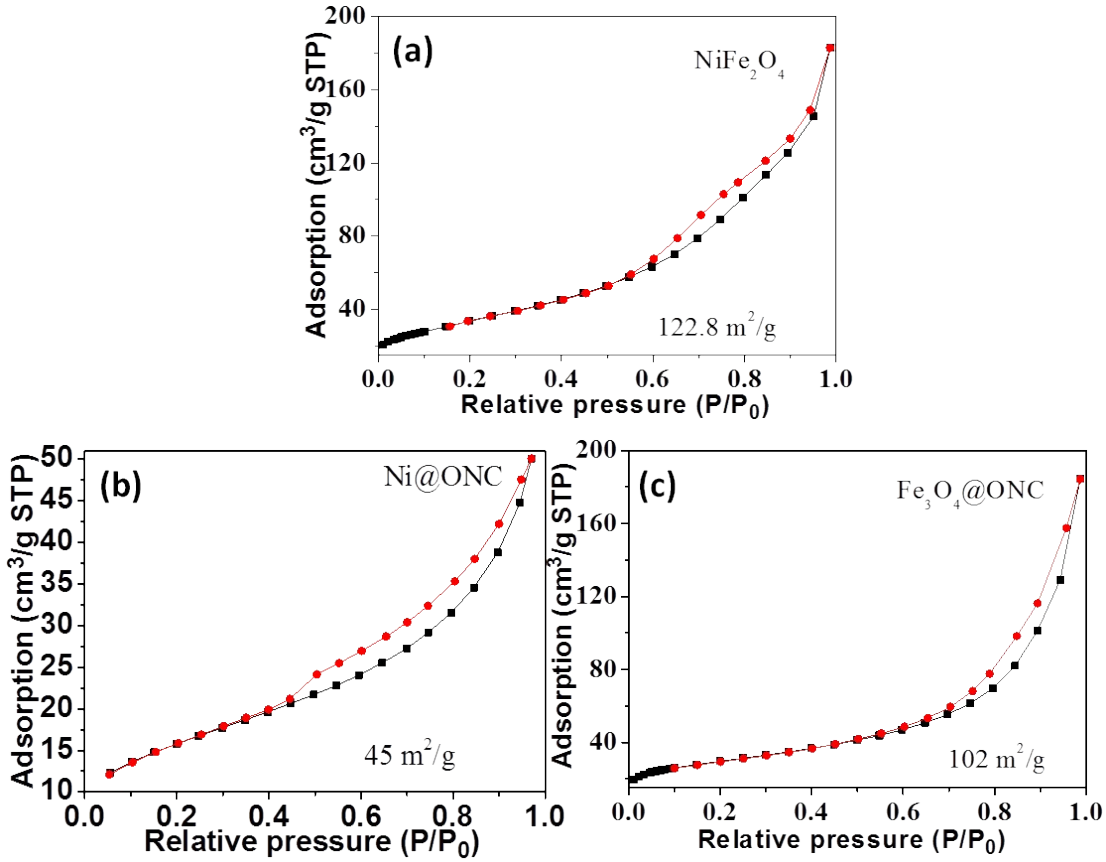

Figure S6. N_2 adsorption-desorption isotherms of (a) $NiFe_2O_4$; (b) Ni@ONC and (c) Fe_3O_4@ONC nanorods.

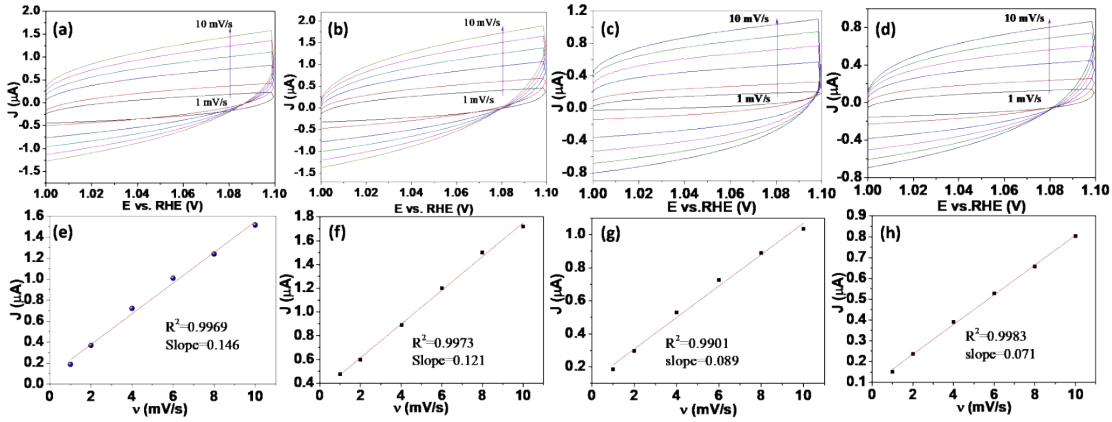

Figure S7. CVs measured at different scan rates from 1 to 10 mV/s for (a) Ni/Fe_3O_4@ONC, (b) $NiFe_2O_4$, (c) Ni@ONC and (d) Fe_3O_4@ONC nanorods and the corresponding plots of current density at 1.08 V versus scan rate for (e) Ni/Fe_3O_4@ONC, (f) $NiFe_2O_4$, (g) Ni@ONC, (h) Fe_3O_4@ONC nanorods, and respectively.

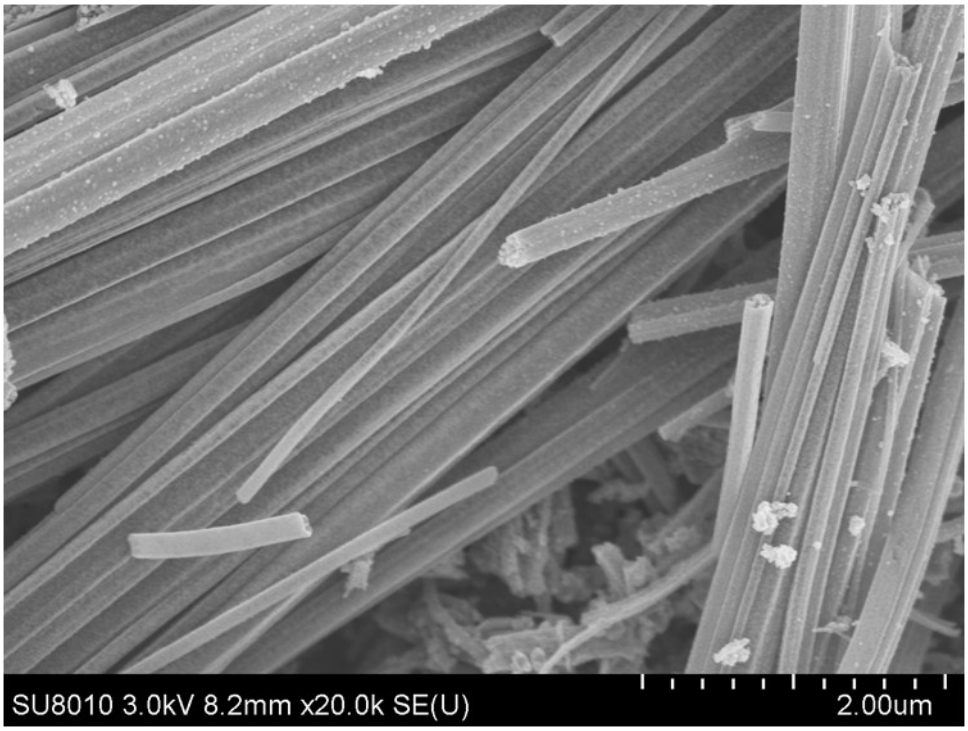

Figure S8. SEM image of post-OER Ni/Fe_3O_4@ONC nanorods.

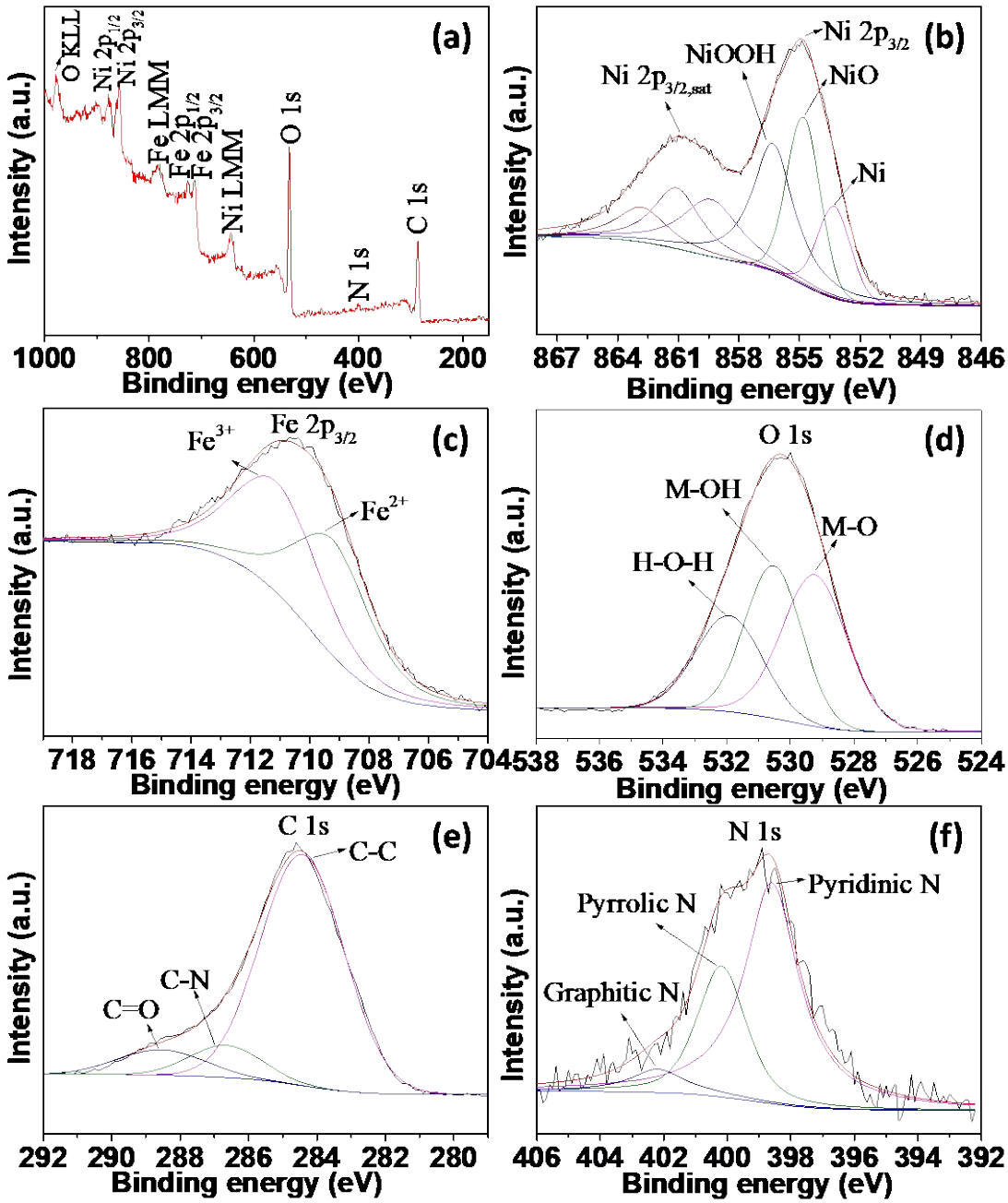

Figure S9. (a) XPS survey spectrum and high-resolution XPS spectrum of (b) Ni 2p, (c) Fe 2p, (d) O 1s, (e) C 1s and (f) N 1s for the post-OER Ni/Fe_3O_4@ONC nanorods.

Table S1. Comparison of the OER activity of Ni/Fe_3O_4@ONC nanorods to several recently reported state of the art OER catalysts.

Catalyst	Substrate	Mass loading (mg/cm^2)	Overpotential@ 10 mA/cm^2 (mV vs. RHE)	Tafel slope ($mV\ dec^{-1}$)	Electrolyte	Reference
Ni/Fe_3O_4@ONC	GC*	0.20	296	61	1M KOH	This work
RuO_2	GC	0.20	348	80	1M KOH	This work
FeNi@NCs	GC	0.32	280	70	1M NaOH	S[1]
Fe-mCo_3O_4	GC	--	380	60	1M KOH	S[2]
Fe_3O_4-Co_9S_8/rGO	GC	0.25	320	54.5	1M KOH	S[3]
$Ni_{0.9}Fe_{0.1}O_x$	QCM electrodes	~0.012	336	30	1M KOH	S[4]
$CoFe_2O_4$	GC	0.285	314	30.69	1M KOH	S[5]
$Fe_{0.1}Ni_{0.9}O$	QCM electrodes	~0.09	297	37	0.5M KOH	S[6]
NiFe-LDH	GC	0.20	350	47	0.1M KOH	S[7]
Fe-Ni/O_x	GC	0.28	299	39	1M KOH	S[8]
$CoFe_2O_4$	CFP	--	378	73	1M NaOH	S[9]
Co-Fe-O/rGO	GC	0.10	340	31	1M KOH	S[10]
NiO/$NiFe_2O_4$	GC	0.12	302	42	1M KOH	S[11]
NiO/$NiFe_2O_4$	CP*	1.0	303	58.5	1M KOH	S[12]

* GC denotes as glassy carbon, CP denotes as carbon paper.

References

1. X. Cui, P. Ren, D. Deng, J. Deng and X. Bao, *Energy Environ Sci*, 2016, **9**, 123-129.
2. C. Xiao, X. Lu and C. Zhao, *Chem Commun*, 2014, **50**, 10122-10125.
3. J. Yang, G. Zhu, Y. Liu, J. Xia, Z. Ji, X. Shen and S. Wu, *Adv Funct Mater*, 2016, **26**, 4712-4721.
4. L. Trotochaud, J. K. Ranney, K. N. Williams and S. W. Boettcher, *J Am Chem Soc*, 2012, **134**, 17253-17261.
5. Y. Liu, J. Li, F. Li, W. Li, H. Yang, X. Zhang, Y. Liu and J. Ma, *J Mater Chem A*, 2016, **4**, 4472-4478.
6. K. Fominykh, P. Chernev, I. Zaharieva, J. Sicklinger, G. Stefanic, M. Doblinger, A. Muller, A. Pokharel, S. Bocklein, C. Scheu, T. Bein and D. Fattakhova-Rohlfing, *ACS Nano*, 2015, **9**, 5180-5188.
7. K. Yan, T. Lafleur, J. Chai and C. Jarvis, *Electrochem Commun*, 2016, **62**, 24-28.
8. L. X. Wang, J. Geng, W. H. Wang, C. Yuan, L. Kuai and B. Y. Geng, *Nano Res*, 2015, **8**, 3815-3822.
9. A. Kargar, S. Yavuz, T. K. Kim, C.-H. Liu, C. Kuru, C. S. Rustomji, S. Jin and P. R. Bandaru, *ACS Appl Mater Interfaces*, 2015, **7**, 17851-17856.
10. J. Geng, L. Kuai, E. Kan, Q. Wang and B. Geng, *ChemSusChem*, 2015, **8**, 659-664.
11. G. Liu, X. Gao, K. Wang, D. He and J. Li, *Int J Hydrogen Energy*, 2016, **41**, 17976-17986.
12. B. K. Kang, M. H. Woo, J. Lee, Y. H. Song, Z. Wang, Y. Guo, Y. Yamauchi, J. H. Kim, B. Lim and D. H. Yoon, *J Mater Chem A*, 2017, **5**, 4320-4324.